NAD^+ supplementation normalizes key Alzheimer's features and DNA damage responses in a new AD mouse model with introduced DNA repair deficiency

Yujun Hou[a], Sofie Lautrup[a,b], Stephanie Cordonnier[a], Yue Wang[c], Deborah L. Croteau[a], Eduardo Zavala[a], Yongqing Zhang[d], Kanako Moritoh[e], Jennifer F. O'Connell[f], Beverly A. Baptiste[a], Tinna V. Stevnsner[b], Mark P. Mattson[c,g], and Vilhelm A. Bohr[a,h,1]

[a]Laboratory of Molecular Gerontology, National Institute on Aging, National Institutes of Health, Baltimore, MD 21224; [b]Danish Aging Research Center, Department of Molecular Biology and Genetics, University of Aarhus, 8000 Aarhus C, Denmark; [c]Laboratory of Neurosciences, National Institute on Aging, National Institutes of Health, Baltimore, MD 21224; [d]Laboratory of Genetics and Genomics, National Institute on Aging, National Institutes of Health, Baltimore, MD 21224; [e]Laboratory of Molecular Biology and Immunology, National Institute on Aging, National Institutes of Health, Baltimore, MD 21224; [f]Laboratory of Clinical Investigation, National Institute on Aging, National Institutes of Health, Baltimore, MD 21224; [g]Department of Neuroscience, Johns Hopkins University School of Medicine, Baltimore, MD 21205; and [h]Danish Center for Healthy Aging, University of Copenhagen, 2200 Copenhagen, Denmark

Edited by James E. Cleaver, University of California, San Francisco, CA, and approved January 5, 2018 (received for review October 30, 2017)

Emerging findings suggest that compromised cellular bioenergetics and DNA repair contribute to the pathogenesis of Alzheimer's disease (AD), but their role in disease-defining pathology is unclear. We developed a DNA repair-deficient 3xTgAD/Polβ$^{+/-}$ mouse that exacerbates major features of human AD including phosphorylated Tau (pTau) pathologies, synaptic dysfunction, neuronal death, and cognitive impairment. Here we report that 3xTgAD/Polβ$^{+/-}$ mice have a reduced cerebral NAD^+/NADH ratio indicating impaired cerebral energy metabolism, which is normalized by nicotinamide riboside (NR) treatment. NR lessened pTau pathology in both 3xTgAD and 3xTgAD/Polβ$^{+/-}$ mice but had no impact on amyloid β peptide (Aβ) accumulation. NR-treated 3xTgAD/Polβ$^{+/-}$ mice exhibited reduced DNA damage, neuroinflammation, and apoptosis of hippocampal neurons and increased activity of SIRT3 in the brain. NR improved cognitive function in multiple behavioral tests and restored hippocampal synaptic plasticity in 3xTgAD mice and 3xTgAD/Polβ$^{+/-}$ mice. In general, the deficits between genotypes and the benefits of NR were greater in 3xTgAD/Polβ$^{+/-}$ mice than in 3xTgAD mice. Our findings suggest a pivotal role for cellular NAD^+ depletion upstream of neuroinflammation, pTau, DNA damage, synaptic dysfunction, and neuronal degeneration in AD. Interventions that bolster neuronal NAD^+ levels therefore have therapeutic potential for AD.

Alzheimer's disease | DNA repair | aging | NAD supplementation | nicotinamide riboside

Alzheimer's disease (AD) is the most common form of dementia, affecting tens of millions of people worldwide, a number expected to double within 20 y (1). AD is characterized by progressive cognitive impairment (2, 3) resulting from synapse loss and neuronal death in brain regions critical for learning and memory and emotional control. The accumulation of two self-aggregating proteins, extracellular amyloid β peptide (Aβ; amyloid plaques) and intracellular phosphorylated Tau (pTau; neurofibrillary tangles) are diagnostic hallmarks of AD (reviewed in ref. 4). Aβ and pTau pathologies are associated with neuroinflammation characterized by activation of microglia and astrocytes and elevated levels of proinflammatory cytokines such as TNFα (5).

Dysfunctional mitochondria are a hallmark of many neurodegenerative diseases, including AD, and a contributing factor may be NAD^+ depletion, which is also observed with aging (the major AD risk factor) in several organisms, including humans (6). NAD^+ is a cellular metabolite, which is critical for mitochondrial health and biogenesis, stem cell self-renewal, and neuronal stress resistance (reviewed in ref. 7). It functions as an essential cofactor for the DNA repair protein PARP1, for deacetylases in the sirtuin family, and for the activity of the cyclic ADP ribose hydrolases CD38 and CD157 (8, 9). The NAD^+-consuming enzymes compete for a limited pool of NAD^+ and therefore may limit each other's activity within the cell if the bioavailability of NAD^+ decreases (10). Since neurons have a relatively high energy demand, they are very sensitive to NAD^+ depletion and impairment of ATP production (6, 11). In addition, NAD^+ affects neuronal health and survival through maintenance of the balance between mitochondrial biogenesis and mitophagy (11, 12). Supplementation with NAD^+ precursors like nicotinamide riboside (NR), nicotinamide mononucleotide (NMN), and nicotinamide (NAM) ameliorates some age-related pathological phenotypes of neurodegenerative diseases (13–16) and attenuates pathological phenotypes in mouse models of premature aging caused by mutations of DNA repair enzymes (11, 12, 17). Also, health improvement and lifespan extension after NAD^+ replenishment have been observed in both *Caenorhabditis elegans* and mice (12, 18). However, the role of NAD^+ in AD is still unclear.

Multiple lines of evidence suggest important roles for impaired neuronal bioenergetics and DNA repair deficiency in AD initiation and progression. Increased damage to nuclear and mitochondrial

Significance

Alzheimer's disease (AD) is the most common form of dementia, and there is no cure. DNA repair activity is deficient in AD patient brains, especially DNA polymerase β (Polβ), a key protein in DNA base excision. NAD^+ is a cellular metabolite critical for mitochondrial health and biogenesis, stem cell self-renewal, and neuronal stress resistance. This study shows that NAD^+ levels were decreased in a new AD mouse model with introduced DNA repair deficiency (3xTgAD/Polβ$^{+/-}$), and NAD^+ supplementation with nicotinamide riboside significantly normalized neuroinflammation, synaptic transmission, phosphorylated Tau, and DNA damage as well as improved learning and memory and motor function. This has implications for human AD intervention.

Author contributions: Y.H., S.L., Y.W., D.L.C., T.V.S., M.P.M., and V.A.B. designed research; Y.H., S.L., S.C., Y.W., E.Z., K.M., J.F.O., and B.A.B. performed research; Y.W., D.L.C., and M.P.M. contributed new reagents/analytic tools; Y.H., S.L., S.C., Y.W., D.L.C., E.Z., Y.Z., J.F.O., B.A.B., and V.A.B. analyzed data; and Y.H., S.L., Y.W., D.L.C., T.V.S., M.P.M., and V.A.B. wrote the paper.

The authors declare no conflict of interest.

This article is a PNAS Direct Submission.

Data deposition: The gene expression data has been deposited with Gene Expression Omnibus (accession no. GSE109055).

[1]To whom correspondence should be addressed. Email: vbohr@nih.gov.

This article contains supporting information online at www.pnas.org/lookup/suppl/doi:10.1073/pnas.1718819115/-/DCSupplemental.

DNA has been observed in brains from mild cognitive impairment (MCI) and AD patients (19, 20), and various types of DNA damage have been associated with neurodegeneration (19, 21–23). Oxidative DNA damage is likely the most significant type of DNA damage in AD (4), which is mainly repaired by base-excision repair (BER). Both BER and DNA double-strand break repair, the primary DNA repair pathways in neurons, have been shown to be compromised in AD compared with the normal aging brain (reviewed in refs. 4 and 24). In both pathways, the NAD^+-consuming enzyme PARP1 detects DNA strand breaks. Hyperactivation of PARP1 and decreased NAD^+ are seen in AD brains, suggesting increased DNA damage and/or inefficient DNA repair (25, 26). The primary polymerase involved in BER is DNA polymerase β (Polβ), and studies have shown that neuronal DNA repair is dependent on Polβ (27, 28). In addition, postmortem human brain samples from both MCI and AD patients have reduced BER efficiency, involving reduced DNA Polβ expression and activity (29, 30), suggesting that loss of Polβ occurs early in disease onset. Additional evidence for an important role for Polβ is that Down syndrome patients have reduced Polβ protein levels and are at extraordinarily high risk for AD (31, 32).

Several mouse models that exhibit Aβ plaque and/or pTau pathologies and cognitive deficits have been developed (33, 34). One widely used AD model, the 3xTgAD mouse, expresses mutant forms of human Aβ precursor protein (APP), presenilin-1 that cause early-onset familial AD, and a Tau mutation that causes frontotemporal dementia (33). The 3xTgAD mice develop age-dependent Aβ plaques, intraneuronal Tau tangles, and cognitive deficits but do not exhibit neuronal death (33, 35). To assess the potential impact of DNA damage and repair in the etiology of AD, we crossed a null allele for Polβ into the 3xTgAD mouse to generate the 3xTgAD/$Polβ^{+/-}$ mice. Our earlier studies demonstrate that the 3xTgAD/$Polβ^{+/-}$ mouse accumulates more DNA damage and exhibits neuronal death in brain regions and that it has a defect in olfactory function that resembles the defective olfaction observed in AD patients (35, 36). Thus, the 3xTgAD/$Polβ^{+/-}$ mice appear to recapitulate features of AD in humans better than previously available mouse models of AD (35). Here, we investigate the effects of NAD^+ precursor on pathophysiology and cellular metabolism in 3xTgAD and 3xTgAD/$Polβ^{+/-}$ mice. The results demonstrate that chronic exposure to NR over 3 mo largely reverts the cognitive deficit in adult 3xTgAD/$Polβ^{+/-}$ and 3xTgAD mice. NR specifically enhances long-term potentiation (LTP) in neurons from 3xTgAD/$Polβ^{+/-}$ mice, with lesser effect on neurons from 3xTgAD mice. In addition, NR stimulates neurogenesis and decreases neuroinflammation and oxidative DNA damage. Because recent studies have demonstrated the oral bioavailability and safety of NR in humans (37), our findings provide strong preclinical support for NR intervention in AD patients.

Results

NR Improves Learning and Memory in AD/Polβ Mice. To determine whether NAD^+ depletion contributed to the neuropathology and cognitive impairment in AD mouse models, we treated 16- to 18-mo-old WT, $Polβ^{+/-}$ (Polβ), 3xTgAD (AD), and 3xTgAD/$Polβ^{+/-}$ (AD/Polβ) mice with NR in their drinking water (12 mM) or no NR (vehicle) for 6 mo. During the last 3 mo of the treatment period, behavioral testing and in vivo metabolic analyses were performed, and the mice were then killed, and their brains were processed for various assays (Fig. 1*A*). The NAD^+/NADH ratio was decreased in the cerebral cortex of Polβ, AD, and AD/Polβ mice compared with WT mice (Fig. 1*B*). The lowest NAD^+/NADH ratio was in AD/Polβ mice. NR treatment significantly increased the cerebral cortical NAD^+/NADH ratio in mice of each of the four genotypes (Fig. 1*B*), suggesting that NR enters the brain and boosts cellular NAD^+ levels when administered orally.

To assess whether NR treatment modifies cognitive deficits in AD and AD/Polβ mice, we performed a battery of behavioral tests. In the Morris water maze test, the vehicle-treated AD and AD/Polβ mice exhibited a spatial-learning deficit as indicated by significantly longer goal latency times on training days 5–7, with AD/Polβ mice performing more poorly than each of the other three genotypes, while NR improves learning ability (Fig. 1 *C* and *D* and Fig. S1*A*). In the probe trials, all groups of mice had similar swimming speeds (Fig. S1*B*). Untreated AD and AD/Polβ mice spent less time in the target quadrant and had fewer platform location crossings compared with WT and Polβ mice (Fig. 1 *E* and *F*), indicating impaired memory retention. NR treatment completely reversed the memory-retention deficits in AD and AD/Polβ mice as indicated by time spent in the target quadrant and platform location crossings that were similar to WT mice (Fig. 1 *E* and *F* and Fig. S1 *C* and *D*).

To measure the recognition memory of the mice, the novel-object recognition test was performed. All mice spent a similar period exploring two identical objects (Fig. S1*E*). After a familiar object was replaced by a novel object, untreated AD/Polβ mice spent significantly less time exploring the novel object compared with WT and Polβ mice, and NR treatment reversed this deficit (Fig. 1*G*). We next evaluated the working memory of mice in the Y-maze. AD and AD/Polβ mice exhibited significantly fewer spontaneous alternations in the Y-maze than did WT and Polβ mice, and NR treatment reversed the working-memory deficit in AD and AD/Polβ mice (Fig. 1*H*). Fear conditioning is a Pavlovian test in which a sound and a footshock are paired, such that the animal learns to associate the sound with the shock. On the second day of testing, there were no significant genotype effects in contextual freezing times in untreated mice (Fig. 1*I*). NR treatment had no effect on contextual freezing times in WT, Polβ, or AD mice but significantly increased freezing times in the AD/Polβ mice (Fig. 1*I*). However, in response to the tone (cued test), NR treatment increased cued freezing times in AD/Polβ mice to the WT level (Fig. 1*J*). Collectively, these findings indicate that NR treatment could significantly improve both learning and memory in AD mice and even more profoundly in AD/Polβ mice.

Since decreased cellular NAD^+ levels occur in several different tissues during normal aging, and recent studies demonstrate beneficial effects of NR on muscle strength and endurance (38, 39), we performed tests of neuromuscular function in control and NR-treated mice. In the rotarod test, the latency to falling off the rotarod was shorter in AD and AD/Polβ mice compared with WT mice, and this poor performance was reversed in NR-treated AD and AD/Polβ mice (Fig. S1*F*), indicating increased motor function. In addition, grip strength analysis showed that vehicle-treated AD and AD/Polβ mice had lower grip strength than WT mice, and NR increased grip strength in all groups (Fig. S1*G*). Human AD patients have gait problems (40). To assess whether this was also the case for our AD mice, we used the MotoRater system for gait analysis (Fig. S1*H*). AD/Polβ mice had a trend toward decreased forepaw step length compared with WT mice, while NR treatment significantly improved step length to the WT level (Fig. S1*I*). In AD/Polβ mice, there were trends for decreased gait speed and increased variance in step length. After NR both parameters were restored almost to WT levels (Fig. S1 *J* and *K*).

AD patients often exhibit increased anxiety and depression (41), and it was previously reported that 3xTgAD mice also exhibit increased anxiety compared with WT mice (42). Here, we found that AD and AD/Polβ mice displayed decreased distance traveled and fewer center entries in the open field; however, NR treatment did not reverse this anxiety-like phenotype in the open-field test (Fig. S2 *A* and *B*). To further evaluate anxiety, we tested all mice in the elevated plus maze. Compared with WT mice, AD/Polβ mice spent less time exploring and had significantly fewer entries into the open arms compared with closed arms, and NR treatment reversed this anxiety-like behavior (Fig. S2 *C* and *D*). To evaluate depression-like behavior, mice were subjected to a forced swim test. We found that AD and AD/Polβ mice showed less immobile time than WT mice (Fig. S2 *E* and *F*), suggesting that the AD mouse models used in this study do

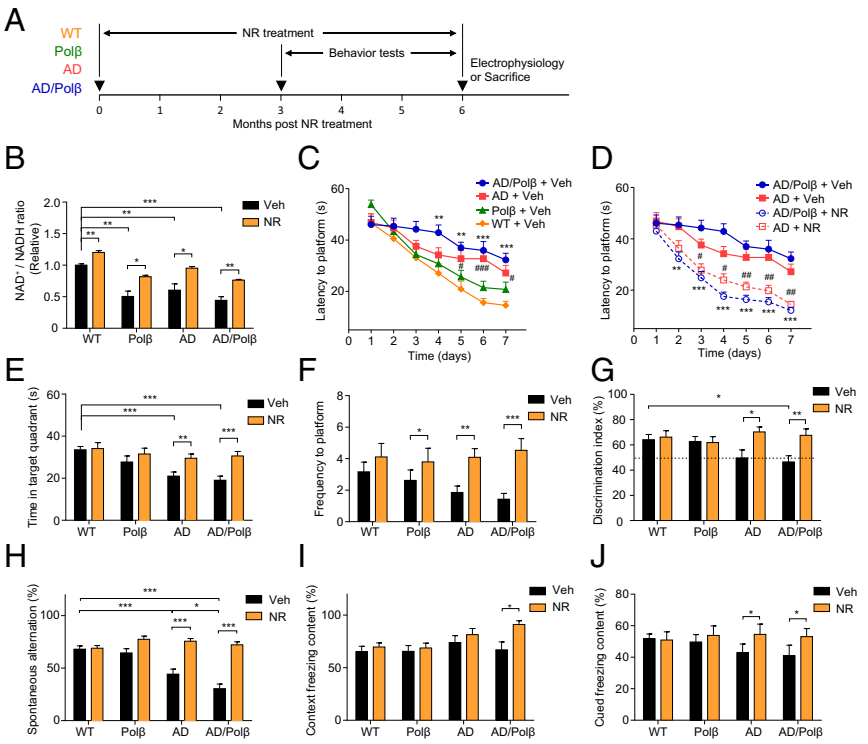

Fig. 1. NR improves learning and memory in AD/Polβ mice. (*A*) Experimental design for NR treatment in WT, Polβ, AD, and AD/Polβ mice. (*B*) Effects of NR supplementation on the NAD^+/NADH ratio in cortex tissue of WT, Polβ, AD, and AD/Polβ mice. (*C* and *D*) Effects of NR supplementation on the learning of vehicle- or NR-treated WT, Polβ, AD, and AD/Polβ mice measured by Morris water maze test. For *C*, $^{**}P < 0.01$, $^{***}P < 0.001$, AD/Polβ versus WT; $^{\#}P < 0.05$, $^{\#\#\#}P < 0.001$, AD versus WT. For *D*, $^{**}P < 0.01$, $^{***}P < 0.001$, NR versus vehicle in AD/Polβ; $^{\#}P < 0.05$, $^{\#\#}P < 0.01$, NR versus vehicle in AD; two-way ANOVA with Tukey's post hoc test. (*E* and *F*) Time in target quadrant (*E*) and frequency of platform location (*F*) in the probe trial of the Morris water maze test in WT, Polβ, AD, and AD/Polβ mice. (*G*) Effects of NR in object-recognition test in WT, Polβ, AD, and AD/Polβ mice with two different objects. (*H*) Effects of NR on the SAP changes in the Y-maze test in WT, Polβ, AD, and AD/Polβ mice. For *B–H*, $n = 17$ (WT + Veh), 16 (Polβ + Veh), 16 (AD + Veh), 16 (AD/Polβ + Veh), 13 (WT + NR), 12 (Polβ + NR), 14 (AD + NR), and 15 (AD/Polβ + NR) mice. (*I* and *J*) Effects of NR on fear memory in the context (*I*) or cued (*J*) fear conditioning test in WT, Polβ, AD, and AD/Polβ mice. $n = 15$ (WT + Veh), 15 (Polβ + Veh), 10 (AD + Veh), 9 (AD/Polβ + Veh), 13 (WT + NR), 12 (Polβ + NR), 10 (AD + NR), and 9 (AD/Polβ + NR) mice. Data are shown as mean ± SEM. $^{*}P < 0.05$, $^{**}P < 0.01$, $^{***}P < 0.001$.

not exhibit depressive behavior. NR normalized the latency to immobility but not immobility time. In summary, NR increased performance on the rotarod, grip strength, and gait function tests and decreased anxiety-like but not depression-like behaviors in AD and AD/Polβ mice. The summary of NR's effects on behavioral phenotypes and others in AD and AD/Polβ are shown in Table S1.

NR Restores Hippocampal Synaptic Plasticity in AD/Polβ Mice. Gene-expression analysis can provide unbiased insights into signaling pathways that are altered by treatment. Here we used parametric analysis of gene set enrichment (PAGE) (43) of curated canonical pathways from BioCarta, Kyoto Encyclopedia of Genes and Genomes (KEGG) (44), and Reactome (45) to identify significantly changed pathways in the hippocampus and cortex following NR treatment. Significantly changed pathways were defined as those displaying an absolute z-score of at least 1.5, a P value ≤ 0.05, and a false-discovery rate (FDR) ≤ 0.3 and having at least three changed genes in the pathway in at least one genotype. By use of heatmaps (Fig. 2 *A* and *B* and Fig. S3 *A* and *B*), we show each genotype (AD, AD/Polβ, Polβ, WT) with vehicle (Veh) or NR treatment, all relative to WT vehicle-treated mice, and a within-genotype comparison, i.e., AD/Polβ (NR) versus AD/Polβ (Veh).

Using these selection criteria, we identified 80 (9.6%) pathways in the hippocampus and 54 (6.5%) in the cortex that are altered after NR treatment (Fig. 2 *A* and *B* and Fig. S3 *A* and *B*). In both brain compartments, immune-related pathways were the most abundant, representing 45% of the pathways from the hippocampus and 31% of the pathways from cortex (Fig. 2*A* and Fig. S3*A*). Multiple pathways related to chemokines, cytokines including interleukins and Toll-like receptors, were seen in both the hippocampus and cortex. In the hippocampus, the direction of change of the immune pathways in AD mice after NR was more similar to Polβ mice, while AD/Polβ mice clearly responded differently (Fig. 2*A*). These results suggest that NR may suppress inflammatory processes robustly in both the hippocampus and cortex.

In the hippocampus, among the nonimmune pathways of NR versus vehicle (Fig. 2*B*), pathways related to neurotrophins and synapse function were uniquely up-regulated in NR-treated AD/Polβ mice. The neurotransmitters pathway was also significantly up-regulated in AD/Polβ after NR treatment. NR produced a more unified response among the genotypes in the cortex than seen in the hippocampus (Fig. S3*B*). P53 signaling was universally down-regulated after NR in all genotypes in the cortex. In contrast to WT, insulin- and ribosome-related pathways were uniformly up-regulated in the AD models and Polβ mice after NR treatment (Fig. S3*B*).

The hippocampus plays a critical role in spatial learning and memory, and its neuronal circuits are damaged in AD. Because NR ameliorated spatial-learning deficits in AD and AD/Polβ mice, and microarray showed that some neurotransmitters and synapse function-related pathways changed in response to NR, we next determined whether NR treatment could improve hippocampal synaptic plasticity. We performed field potential recordings at the CA1 stratum radiatum in hippocampal slices from ~22-mo-old WT mice, vehicle-treated, and NR-treated AD and AD/Polβ mice (Fig. 2*C*). We measured LTP, a classic measure of synaptic plasticity

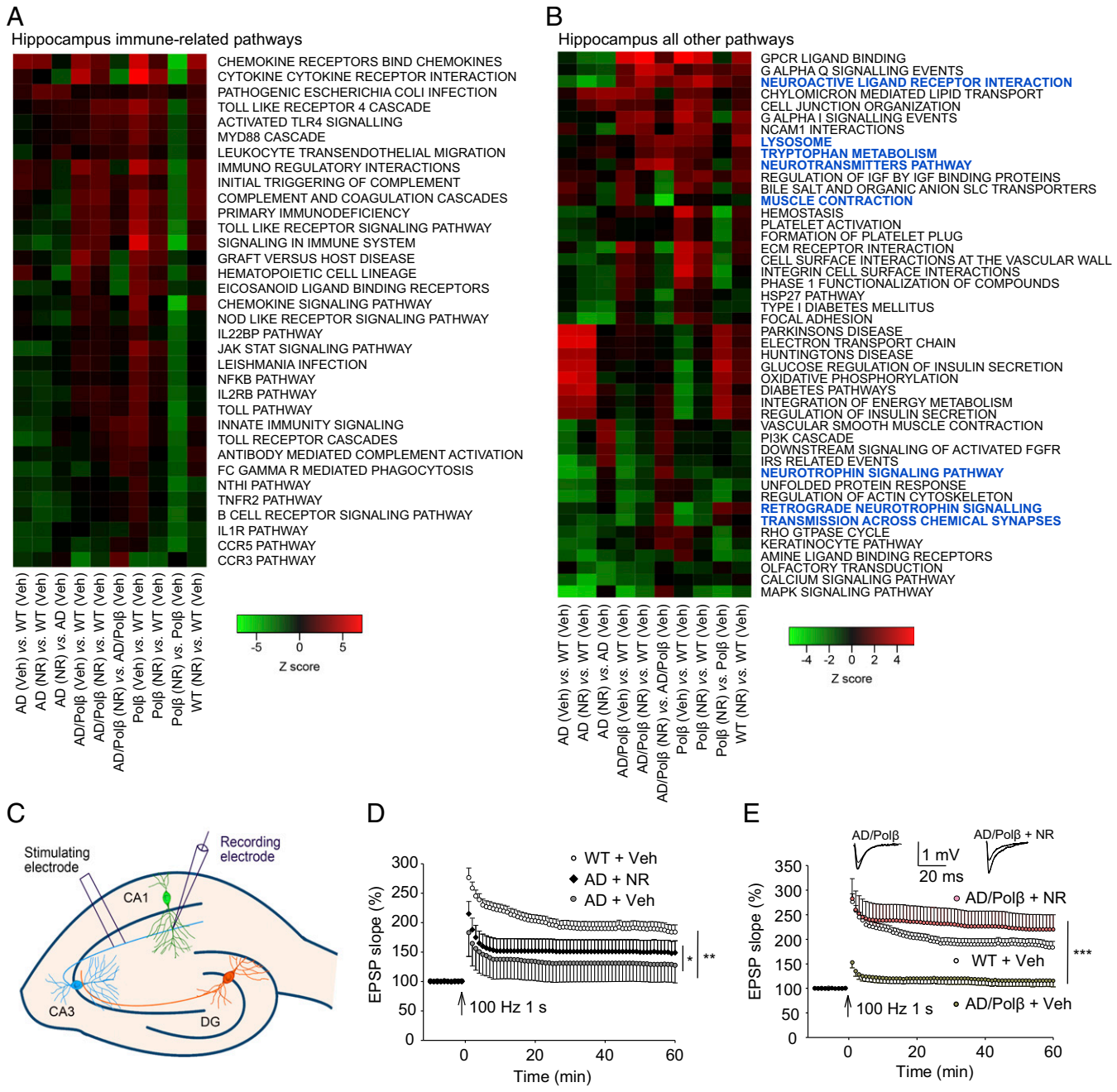

Fig. 2. NR improves long-term potentiation. (*A* and *B*) Pathways in the hippocampi of NR- and vehicle-treated mice of each genotype were compared. Pathways that showed ≥1.5-fold change in at least one genotype are shown. We have fixed the order of the samples but allowed the clustering of the pathways based on row means. In hippocampus, immune-related pathways were the most abundant. We divided the pathways into immune-related pathways (*A*) and all other pathways (*B*). Blue color indicates the pathways related to neurotransmitters, synaptic function, muscle contraction, and so forth. (*C*) Illustration showing locations of the stimulating and recording electrodes for electrophysiological analyses of synaptic transmission at CA1 neuron synapses. (*D* and *E*) Results of analyses of LTP measured at the Schaffer collateral synapses. For *D* and *E*, values are the mean and SEM of determinations made on eight hippocampal slices from at least five different mice. EPSP, excitatory postsynaptic potential. $*P < 0.05$, $**P < 0.01$, $***P < 0.001$.

involved in learning and memory (46). Input–output analysis revealed no significant differences in basal synaptic transmission among the five groups of mice (Fig. S3 *C* and *D*), as reported previously (35). Paired-pulse facilitation analysis was performed to determine whether the neurotransmitter (glutamate) release from presynaptic terminals was affected by genotype or NR, and it was similar in all five groups of mice (Fig. S3 *E* and *F*). Whereas robust LTP was induced by high-frequency stimulation in slices from WT mice, LTP was markedly impaired in slices from AD mice (Fig. 2*D*). We show that the magnitude of LTP was significantly greater in slices from NR-treated AD mice than control AD mice (Fig. 2*D*). Surprisingly, whereas LTP was essentially absent in slices of AD/Polβ mice, it was dramatically restored to normal levels in NR-treated AD/Polβ mice (Fig. 2*E*), which showed that NR can improve synaptic function.

NR Increases Neurogenesis and Decreases Neuroinflammation. Adult hippocampal neurogenesis plays important roles in dentate gyrus

(DG)-dependent types of learning and memory and has been reported to be compromised in AD (47). To quantify newly generated neurons arising from neural progenitor cells (NPCs), we derived NPCs from embryonic mouse cortex. As shown in Fig. 3*A*, more than 90% of the cells in the culture were identified as $Sox2^+$ NPCs. EdU is incorporated into newly synthesized DNA in proliferating cells. We found that 40% of total cells were EdU^+ in vehicle-treated cells. NR treatment (1 mM) for 24 h resulted in a significant increase of EdU incorporation in NPCs (Fig. 3 *A* and *B*), demonstrating that NR increases proliferation of NPCs.

In AD patients, abnormal neuroinflammation is associated with Aβ neuritic plaques and is characterized by activation of microglia and proinflammatory cytokine production (5). Our microarray analysis revealed up-regulation of inflammation-related pathways in AD and AD/Polβ mice and suppression of inflammation-related pathways by NR treatment. We therefore evaluated multiple markers of neuroinflammation in mouse brain sections. Signals from the marker for activated astrocytes, GFAP, and for the microglia marker IBA1 were dramatically increased in both hippocampus and cortex regions of AD/Polβ and AD mice, with AD/Polβ mice exhibiting more activated astrocytes and microglia than AD mice (Fig. 3 *C*–*F*). NR treatment decreased the activated astrocytes and microglia in AD and especially in AD/Polβ mice (Fig. 3 *C*–*F*). Since activated astrocytes and microglia produce proinflammatory cytokines that likely contribute to AD pathology and cognitive impairment, we quantified several cytokine and chemokine levels in plasma samples from control and NR-treated mice. AD/Polβ mice had elevated levels of proinflammatory cytokines and chemokines, including IL-1α, TNFα, MCP-1, IL-1β, MIP-1α, and RANTES, and decreased levels of antiinflammatory cytokines such as IL-10 (Fig. 3*G* and Fig. S4*A*). NR treatment of AD/Polβ mice normalized the levels of these cytokines to WT (Fig. 3*G*). Collectively, these results demonstrate that NR treatment suppresses brain and systemic inflammation in AD/Polβ mice.

Changes in immune cell populations are known to occur in AD mice (48). To assess the immune cell population changes in

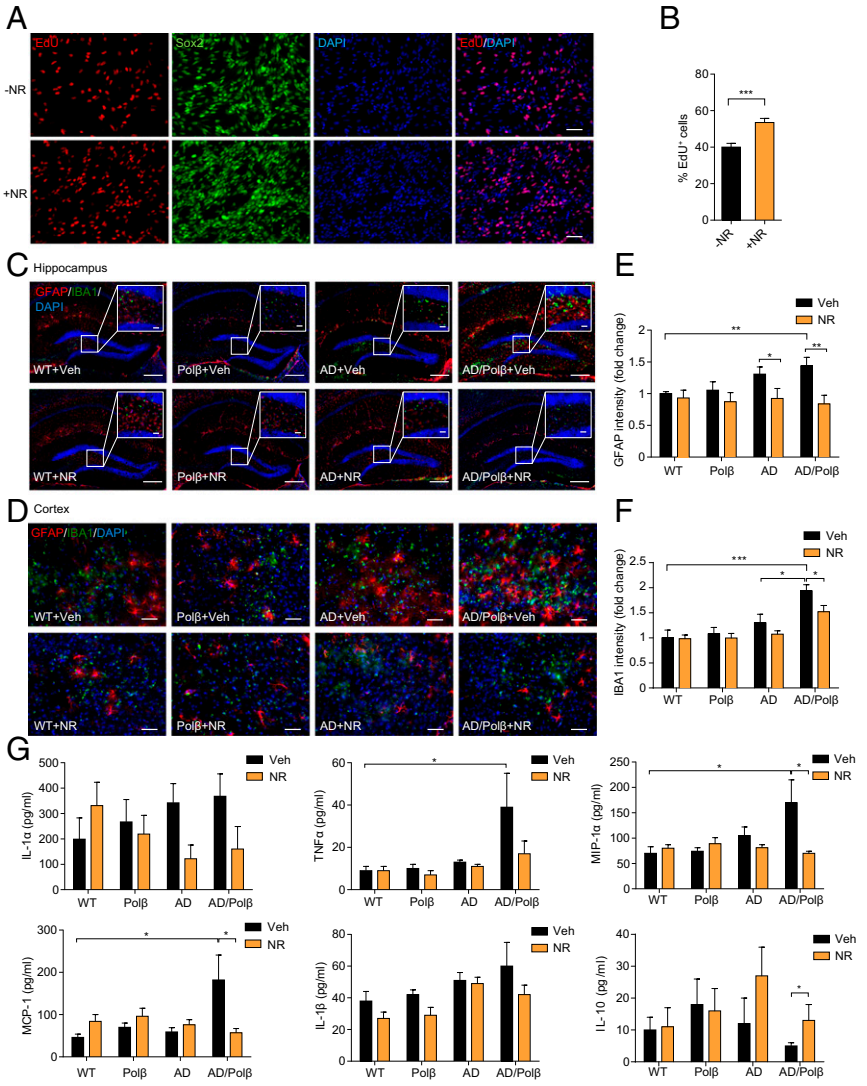

Fig. 3. NR increases in vitro EdU incorporation in NPCs and decreases neuroinflammation. (*A*) Representative images of EdU (red), Sox2 (green), and DAPI (blue) staining of NPCs treated with vehicle or 1 mM NR for 24 h. (Scale bars, 50 μm.) (*B*) Quantification of EdU^+ cells from images as in *A*. $n = 27$ control (−NR) and 26 +NR images in three experiments. (*C* and *D*) Representative images of GFAP (red) and IBA1 (green) staining of hippocampus regions (*C*) and cortex regions (*D*) from WT, Polβ, AD, and AD/Polβ mice treated with vehicle or NR. (Scale bars: 200 μm in *C*; 20 μm in *C*, *Inset*; 50 μm in *D*.) (*E* and *F*) Quantification of GFAP (*E*) and IBA1 (*F*) intensity from sections as in *C* and *D*. $n = 5$ mice per group. Quantifications are presented as mean ± SEM. (*G*) Indicated cytokine or chemokine levels in mouse plasma detected by multiplex cytokine array. $n = 11$ (WT + Veh), 10 (Polβ + Veh), 11 (AD + Veh), 12 (AD/Polβ + Veh), 9 (WT + NR), 10 (Polβ + NR), 8 (AD + NR), and 9 (AD/Polβ + NR) mice. Quantifications are presented as mean ± SEM. $^*P < 0.05$, $^{**}P < 0.01$, $^{***}P < 0.001$.

spleen, we isolated single cells from spleens of vehicle- or NR-treated animals and analyzed the cell population by flow cytometry. T and B cells ($CD4^+$, $CD8^+$, and $CD19^+$, respectively), macrophages ($CD11b^+$), and dendritic cells ($CD11c^+$) were identified. The AD/Polβ mice showed increased $CD4^+$ T cells, while AD mice showed a marked increase in $CD8^+$ T cells (Fig. S4 *B* and *C*). NR-treated AD/Polβ and AD mice showed levels of immune cells similar to WT mice. $CD19^+$ T cells, macrophages and dendritic cells in spleen were not significantly changed between AD and AD/Polβ mice (Fig. S4 *D*–*F*). These results suggest that NR can restore abnormal immune responses in AD/Polβ and AD mice.

NR Decreases Tau Phosphorylation but Not Aβ Accumulation in AD and AD/Polβ Mice. The accumulation of pTau protein in neurons produces neurotoxic tangles, leading to neuronal dysfunction. Several phosphorylation sites of Tau have been identified in neuronal cells of AD patients, including Thr^{181}, Ser^{202}/Thr^{205}, and Thr^{231}, and these are considered clinical biomarkers of AD (49). Therefore, we investigated whether NR affects Tau phosphorylation. We immunostained mouse brains for Tau–$pThr^{231}$ (50). AD and AD/Polβ mice showed higher levels of pTau in the hippocampus and cortex compared with WT mice, and NR-treated AD and AD/Polβ mice showed significantly decreased pTau levels (Fig. 4 *A*–*C*). Total tau and pTau isoforms were assessed by immunoblot in hippocampal tissue, and AD and AD/Polβ mice showed increased levels compared with WT mice. Notably, NR treatment dramatically decreased pTau levels and the pTau/total Tau ratio at all sites in AD/Polβ mice (Fig. 4*D* and Fig. S5). NR also decreased pTau levels but did not decrease the ratio of pTau/total Tau in the hippocampi of AD mice (Fig. 4*D* and Fig. S5). Thus, NR decreases the accumulation of hyperphosphorylated Tau in the brain of AD/Polβ mice.

We next performed ELISAs to quantify levels of soluble and insoluble $A\beta_{40}$ and $A\beta_{42}$ in hippocampal tissue samples from all mice. No significant differences of soluble and insoluble $A\beta_{40}$ and $A\beta_{42}$ were found between control and NR-treated AD and AD/Polβ mice (Fig. S6*A*). NR treatment also did not affect the density of Aβ plaques in AD and AD/Polβ mice measured by immunofluorescence (Fig. S6 *B* and *C*). To examine whether NR could decrease Aβ expression in vitro, we measured $A\beta_{40}$ and $A\beta_{42}$ levels in SH-SY5Y human neuroblastoma cells overexpressing APP with the Swedish mutation. Treatment with 0.15–15 mM NR for 24 h did not change $A\beta_{40}$ and $A\beta_{42}$ levels and did not affect cell viability (Fig. S6 *D* and *E*). These results show that NR does not affect Aβ production or Aβ plaque formation, suggesting that the beneficial effects of NR on cognition and pTau pathology are independent of Aβ pathology in AD and AD/Polβ mice.

NR Normalizes Mitochondrial Stress in Human AD Fibroblasts. Multiple aging, DNA repair, and metabolic pathways converge upon NAD^+ metabolism and mitochondrial function (51). Since AD patients show increased oxidative stress compared with healthy individuals (52), we investigated the oxidative DNA damage using AD patient fibroblasts (AG07374) and fibroblasts from age-matched controls (AG09857). 8-Hydroxy-2′-deoxyguanosine (8-oxo-dG) is one of the most abundant oxidative DNA lesions (53). Human AD fibroblasts treated with 1 mM NR for 24 h

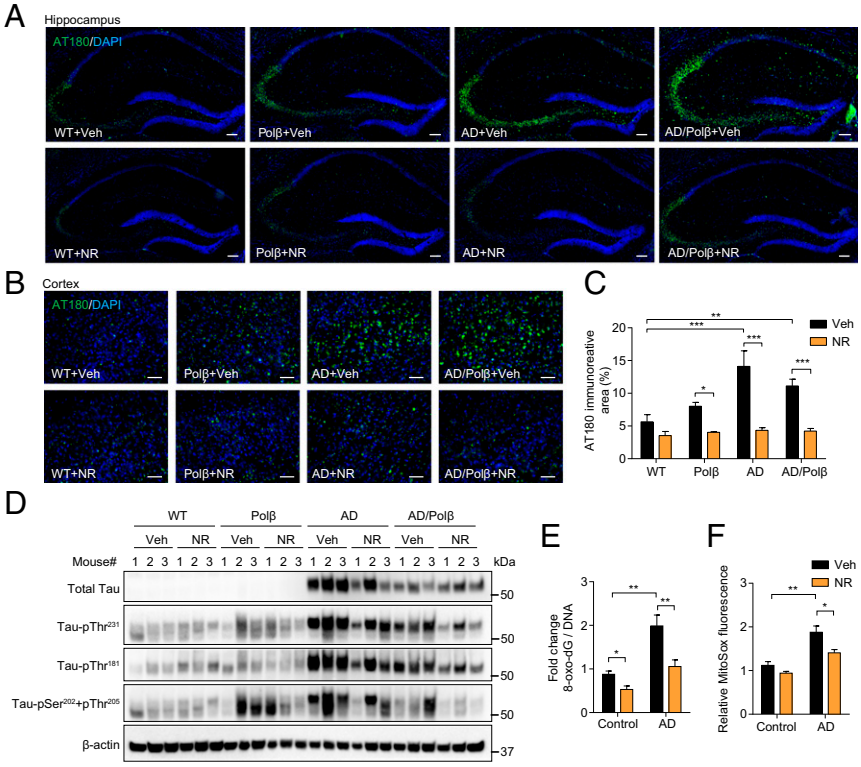

Fig. 4. NR decreases tau phosphorylation in AD/Polβ mice and decreases oxidative damage in human AD fibroblasts. (*A* and *B*) Representative images of AT180 (green) and DAPI (blue) staining of hippocampus regions (*A*) and cortex regions (*B*) from WT, Polβ, AD, and AD/Polβ mice treated with vehicle or NR. (Scale bars, 100 μm.) (*C*) Quantification of the $AT180^+$ immunoreactive area from sections as in *B*. $n = 5$ mice per group. (*D*) Representative immunoblots of the indicated Tau or pTau proteins from the hippocampus of WT, Polβ, AD, and AD/Polβ mice after treatment with vehicle or NR. Quantification of data is shown in Fig. S5. (*E*) ELISA of 8-oxo-dG in AD human fibroblasts and control fibroblasts with or without NR treatment (1 mM for 24 h). (*F*) Mitochondrial superoxide production measured by MitoSOX in AD human fibroblasts and control fibroblasts with or without NR treatment (1 mM for 24 h). For *C*, *E*, and *F*, data are shown as mean ± SEM. $*P < 0.05$, $**P < 0.01$, $***P < 0.001$.

showed a 50% reduction of 8-oxo-dG levels as measured by ELISA (Fig. 4*E*). Mitochondrial reactive oxygen species (ROS) production was also measured using the MitoSOX probe. NR treatment of AD fibroblasts resulted in decreased levels of mitochondrial ROS compared with vehicle-treated cells (Fig. 4*F*). Combined, our results show that NR decreases oxidative damage in human AD fibroblasts.

NR Treatment Decreases DNA Damage and Apoptosis Through SIRT3 and SIRT6. To further explore the underlying beneficial effects of NR, we examined the expression levels of factors important for the mitochondrial stress response in samples of hippocampus from vehicle- and NR-treated WT, Polβ, AD, and AD/Polβ mice. Protein poly ADP ribosylation (PARylation) is a posttranslational modification upon DNA damage, which is catalyzed by poly (ADP ribose) polymerase (PARP). This modification alters many biological processes, including the DNA damage response, transcriptional regulation, and apoptosis (54). PARP1 can be activated by DNA damage and plays an important role in DNA repair. Poly ADP ribose (PAR) was increased in AD and AD/Polβ mice compared with WT mice, and the PAR level decreased dramatically after NR treatment in AD/Polβ mice (Fig. 5 *A* and *B*). PARP1 protein was also lower in NR-treated AD/Polβ mice than in vehicle-treated controls (Fig. 5*A* and Fig. S7). Sirtuins are NAD^+-dependent protein deacetylases. We found that AD/Polβ mice expressed lower levels of SIRT3 and SIRT6 than WT mice, and their expression was restored to WT levels after NR treatment (Fig. 5 *A* and *B*). We then examined the acetylation state of SOD2, an established SIRT3 substrate (55). Acetylated SOD2 and the ratio of acetylated SOD2 to SOD2 in NR-treated AD/Polβ mice was decreased (Fig. 5 *A* and *B*), suggesting that NR treatment increases SIRT3 protein level and deacetylase activity in AD/Polβ mice. As previously reported, we showed that the DNA damage marker γH2AX and apoptosis marker Bcl-2 were increased in AD/Polβ mice (35). Here, we found that NR significantly decreased the abundance of these two markers by Western blot (Fig. 5 *A* and *B* and Fig. S7), suggesting decreased DNA damage and likely increased DNA repair. NR administration significantly reduced the level of DNA damage and apoptosis in both AD and AD/Polβ mice, as detected by immunoreactive γH2AX staining and cleaved-caspase 3 signal in the DG region. Notably, the effect of NR on AD/Polβ mice was more pronounced (Fig. 5 *C* and *D* and Table S1).

Discussion

Our findings document substantial beneficial effects of NR treatment on multiple aspects of neuropathology (pTau, neuroinflammation, and oxidative stress) and on hippocampal synaptic plasticity and cognition in AD and AD/Polβ mice. The DNA repair-deficient AD/Polβ mice show an exacerbation of major AD features and a phenotype more similar to human AD than other AD models (35). The beneficial effects of NR were generally stronger in this mouse than in the 3xTgAD mouse (summarized in Table S1). Specifically, NR shows greater effects on learning and memory, LTP, neuroinflammation, gait function, DNA damage, and sirtuin activity in this DNA repair-defective mouse model. This justifies additional research on the use of NR or other NAD^+ precursors for treating AD in humans.

NR has shown beneficial effects in other DNA repair-deficient disease models, including ataxia-telangiectasia, xeroderma pigmentosum group A, and Cockayne syndrome (11, 12, 17). NAD^+ precursors such as NMN and NAM also improve memory and learning and mitochondrial function and increase lifespan in animal models of AD, Parkinson's disease, and hearing loss (15, 56, 57). This suggests that NAD^+ up-regulation can reverse the impaired brain-energy metabolism and possibly oxidative stress that are implicated in cognitive decline. We found that NR has a dramatic effect on both behavior and neuronal functions, especially in AD/Polβ mice. The defects in learning, memory, and synaptic plasticity are more severe in the AD/Polβ mouse compared with the other AD transgenic mice (35). This suggests that the base-excision DNA repair deficiency exacerbates AD-related deficits in hippocampal synaptic plasticity. We therefore examined how NR intervention affects these parameters and found that both learning and memory were restored significantly, as shown by the Morris water maze, Y maze, and object-recognition tests. Also, synaptic plasticity, measured as LTP, was remarkably increased, especially in the AD/Polβ mouse, after NR treatment. The effect on LTP is supported by previous in vitro findings in NR-treated hippocampal slices from the Tg2576 AD model (57).

Additionally, NR has been shown to have rejuvenation effects on stem cells in both muscle and brain (58). We observe increased neurogenesis after NR treatment, and we detect improved motor function and grip strength, suggesting improved proliferation of NPCs and improved muscle function, potentially via increased muscle stem cell function, as reported recently (18).

Previous studies have shown a decrease in Aβ after NR or NAM treatment (16, 57). In our study, we do not observe an effect of NR on Aβ in the hippocampus or cortex. This may be explained by the different AD model used, as there are relatively few Aβ plaques in our mice compared with other models. This finding could suggest that pathways other than Aβ may contribute more to AD pathogenesis. Here we show a decrease in tau phosphorylation in the hippocampus of both AD and AD/Polβ mice after NR treatment.

SIRT6 is critical for maintaining genomic stability in the brain, and recently it was reported that brain-specific loss of SIRT6 leads to toxic tau stability and phosphorylation (59). Our results showing increased SIRT6 protein and decreased tau phosphorylation after NR are consistent with those findings. Human AD patients show increased inflammation in the brain, as seen by activated astrocytes and microglia (60). NR reduced inflammation in mouse models of diabetes (61, 62). This is confirmed here by microarray analysis and by reduced neuroinflammation in the brain, decreased proinflammatory cytokines, and altered spleen cell types in AD/Polβ mice treated with NR. Increased oxidative DNA damage has been observed in brains of AD patients (23); this may reflect decreased BER activity and increased oxidative stress. Consistent with this, γH2AX abundance was higher in brains of AD/Polβ mice than in brains of control animals, but this was normalized by treatment with NR. This is important because we have previously shown that γH2AX foci accumulate in the hippocampus by 14 mo (35); therefore NR treatment either helped clear preexisting foci or prevented the fixation of new γH2AX foci. In either scenario, NR clearly decreases the load of DNA damage in the hippocampus. Besides mouse studies, we also analyzed human AD fibroblasts in this study. Oxidative DNA damage is increased in these cells (52), and our results confirm this finding, and show that NR can decrease the amount of oxidative DNA damage and mitochondrial oxidative stress.

During aging and at the onset of MCI/AD, oxidative stress and DNA damage increase (4). This leads to DNA strand break-induced depletion of NAD^+ by PARP1. PARylation is increased in human AD patients (63). We show that NR decreases PARylation. Decreased DNA repair and depletion of NAD^+ are critically important, especially to postmitotic cells like neurons. Neurons are highly dependent on DNA repair, since they cannot divide and replace themselves and because of their high energy demand, which leads to increased oxidative stress, likely highest in the mitochondria. This can cause mitochondrial dysfunction, decreased neurogenesis, and neuronal dysfunction, plus increased neuroinflammation, all traits of or contributors to AD, resulting in decreased cognitive abilities (Fig. 5*E*). We show that by increasing cellular levels of available NAD^+ by NR supplementation, we decrease DNA damage, suggesting a link between NAD^+ and BER. Increased NAD^+ enhances the activity of sirtuins, proteins important for the mitochondrial function (7). Previous studies have reported a connection

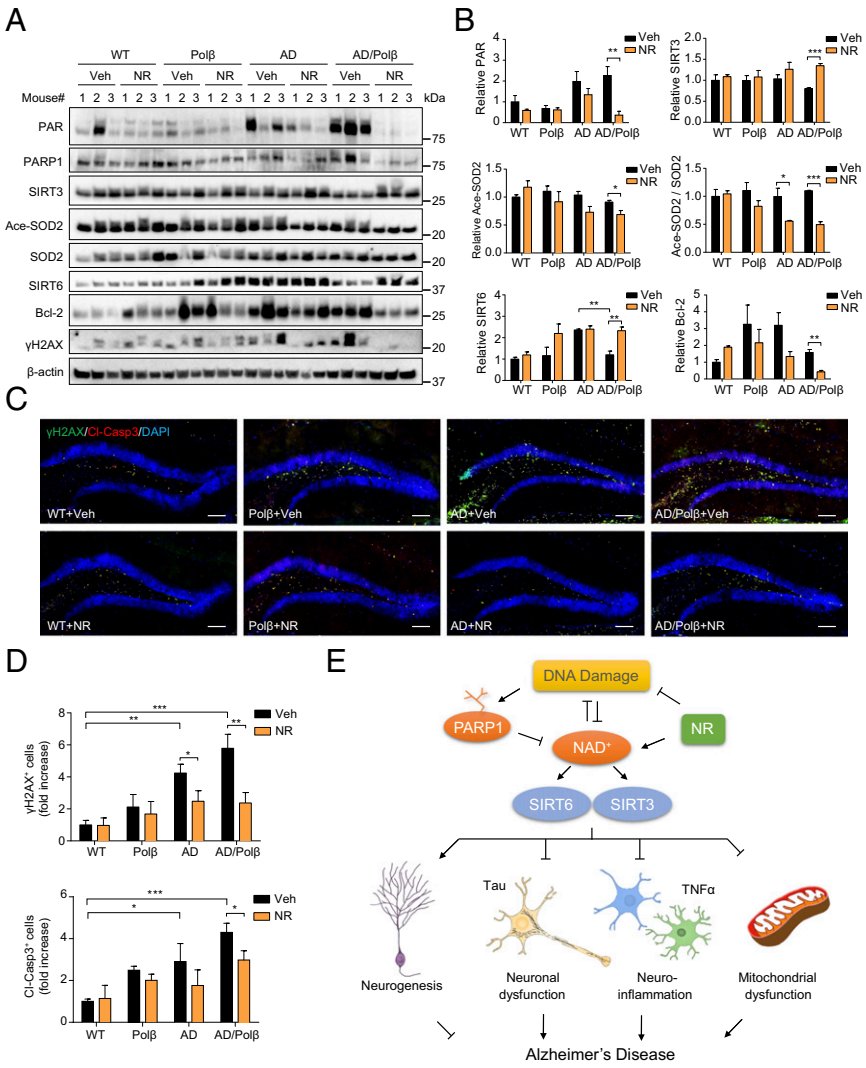

Fig. 5. DNA damage and apoptosis are decreased after NR treatment. (*A*) Representative immunoblots of the indicated proteins from the hippocampus of WT, Polβ, AD, and AD/Polβ mice after treatment with vehicle or NR. Quantifications of data are shown in *B* and Fig. S7. (*B*) Quantification of immunoblots from the indicated proteins in *A*. (*C*) Representative images of γH2AX (green), cleaved-caspase 3 (red), and DAPI (blue) staining of DG sections from WT, Polβ, AD, and AD/Polβ mice treated with vehicle or NR. (Scale bars, 100 μm.) (*D*) Quantification of $\gamma H2AX^+$ cells and cleaved-caspase3$^+$ cells from sections as in *C*. $n = 5$ mice per group. (*E*) Summary figures showing our proposed mechanisms of the relation among NAD^+, DNA damage, sirtuin, and AD. For *B* and *D*, data are shown as mean ± SEM. $^*P < 0.05$, $^{**}P < 0.01$, $^{***}P < 0.001$.

between sirtuins and mitochondrial function, Tau, and Aβ. We observe that NR increases SIRT3 and SIRT6 in our DNA repair-deficient AD mouse model. This study suggests that NR/NAD^+ can target several aspects of AD, including traditional endpoints like Tau pathology and inflammation, maybe via DNA repair enhancement. We believe that this work sets the stage for using NAD^+ for treating AD in humans.

Materials and Methods

Animals. All mice were maintained on a standard NIH diet in a 12-h light/dark cycle. The animals were group housed if possible. All mice were housed in the National Institute on Aging (NIA), Baltimore. All animal experiments were performed using protocols approved by the appropriate institutional animal care and use committee of the NIA. The original AD line was generated as described previously (33). The breeding methods of Polβ and AD/Polβ strains were described previously (35). Both male and female adult mice were used in the experiments with littermate controls used throughout. All experiments were performed blinded using only mouse identification numbers with the exception of Western blot analysis. In animal behavioral studies, animals were randomized in processing order.

NR Supplementation in Mice. WT, Polβ, AD, and AD/Polβ mice (16 to 18 mo old) were given 12 mM NR in their drinking water ad libitum, while the control groups received drinking water without NR. Dosing with NR continued for 3 mo before the start of and throughout behavioral tests (Fig. 1*A*). Water bottles were changed twice a week.

NAD^+ Detection. Mice cortex samples were harvested, and NAD^+ was measured with a commercially available NAD^+/NADH assay kit (no. ab65348; Abcam) according to the manufacturer's protocol.

Morris Water Maze Test. The Morris water maze test was performed as described previously (64). The apparatus was a circular pool (140-cm diameter) filled with water. Tests were performed at 22 °C. The pool was painted with nontoxic white paint. A 12-cm-diameter transparent platform was placed 1 cm below the water surface at a fixed position. Mice were taken to the behavior room, acclimatized, and trained on seven consecutive days, four trials per day. The starting point changed after each trial of a daily training session. Each trial lasted 60 s or until the mouse found the platform. If the platform was not located during the time period, then the mouse was directed to the platform. After each trial, the mouse was placed on the platform for 30 s. On day seven, upon completion of the training phase, the platform was

removed for the probe trial. The duration of probe trial was 60 s and began 1 h after the last training phase. All parameters were recorded semiautomatically by a video tracking system (ANY-Maze; Stoelting).

Object-Recognition Test. Tests were performed as described previously (65). The device was a Plexiglas box (25 × 25 × 25 cm). During the training phase, each mouse could explore two identical objects for 10 min. After 1 h, the mouse was returned to the box, which had been modified to contain one familiar object and one novel object. To exclude olfactory cues, the boxes and objects were cleaned before each test. The automatic tracking system (ANY-Maze; Stoelting) was used to monitor exploration behavior. Exploration time was calculated as the length of time the mouse sniffed or pointed its nose or paws at the object. The preference in the training phase and the recognition index in the testing phase were calculated as follows: "preference" refers to the time spent exploring an object relative to the time spent exploring both objects. The "recognition index" refers to the time spent exploring the novel object relative to the time spent exploring both objects.

Y-Maze Test. The Y-maze Spontaneous Alternation Performance (SAP) test measures the ability of the mice to recognize the environment they had already explored. The maze consisted of three arms (8 × 30 × 15 cm), with an angle of 120° between each arm. The numbers of entries and alterations were recorded using the ANY-Maze tracking system. Mice were introduced at the center of the Y maze and allowed to freely explore the maze for 10 min. The arms were cleaned with 70% ethanol solution between trials. SAP is the subsequent entry into a novel arm over the course of three entries, and the % SAP is calculated by the number of actual alternations/(total arm entries − 2) × 100 (66).

Fear-Conditioning Test. Fear memory is measured by pairing a conditioned stimulus (CS) to an unconditioned stimulus (US) as described previously (67). We used Video Freeze Conditioning software (Med Associates) to measure freezing behavior. On day one, mice were placed inside the chambers; after 120-s baseline, a 30-s CS tone followed, and a US foot shock was given during the last 2 s of the CS. This CS–US pairing was repeated two additional times during 180–220 s and 240–270 s. On day two, both contextual and cued phases were done. During phase one, mice were placed in the same testing chambers used on day one for 5 min. During phase two, 3 h later, mice were placed into modified chambers with plastic inserts, and after 300 s the CS tone was played for 30 s at 1-min intervals (five CS tones in total). After 10 min, mice were returned to their housing cages.

Electrophysiology. Hippocampal slices were prepared as described previously (68). Briefly, the mice were killed using isoflurane gas, the brains were rapidly removed, and transverse slices were cut at a thickness of 350 μm. The slices were allowed to recover for at least 1 h in artificial cerebrospinal fluid (ACSF) at room temperature (RT) before recording. ACSF consisted of 120 mM NaCl, 2.5 mM KCl, 1.25 mM NaH_2PO_4, 26 mM $NaHCO_3$, 1.3 mM $MgSO_4$, 2.5 mM $CaCl_2$, and 10 mM glucose (pH 7.4). The osmolarity of the ACSF was adjusted to 290 milliosmoles using a 5600 Vapor Pressure Osmometer (Wescor, Inc.). Stimuli (30 ms every 20 s) were delivered with a fine bipolar tungsten electrode to activate Schaffer collateral/commissural afferents. LTP was induced with a train of titanic stimulation (100 Hz for 1 s). All recordings were performed at 30–32 °C. Data were collected using a MultiClamp 700B amplifier (Molecular Devices). Signals were filtered at 2 kHz, digitized at 10 kHz with a Digidata 1440A Data Acquisition System, and analyzed using pCLAMP 10 software (Molecular Devices).

Immunofluorescence. Anesthetized mice were perfused with PBS buffer and then with 4% paraformaldehyde (PFA) in PBS. The collected brains were placed in 4% PFA for 24 h and then equilibrated in 30% sucrose for 24 h. A series of equidistant floating 30-μm coronal sections (interval, 240 μm) were prepared, including the DG area. Approximately 9 or 10 slices of each mouse were incubated in blocking buffer (10% donkey serum and 0.3% Triton X-100 in PBS) for 30 min at RT. Thereafter, samples were incubated overnight with the primary antibody at 4 °C and then were incubated with the appropriate fluorescent probe-conjugated secondary antibodies for 1 h at RT. Nuclei were counterstained with DAPI. The entire DG was scanned using an Axiovert 200M Zeiss microscope (Zeiss) equipped with AxioVision 4.8.3.0 software. The number of specific cells was counted using ImageJ software. Specific primary antibodies used include rabbit anti-GFAP (no. Z033401-2; DAKO), mouse anti-6E10 for Aβ (no. 803002; BioLegend), goat anti-IBA1 (no. NB100-1028; Novus), rabbit anti-γH2AX (no. 9719; Cell Signaling Technology), rabbit anti–cleaved-caspase 3 (no. 9579; Cell Signaling Technology), and mouse anti-AT180 for pTau Thr-231 (no. MN1040; Thermo Fisher Scientific).

Cytokine Array. Mouse eye bleeds were collected in EDTA-treated tubes. After centrifugation, the supernatant was flash frozen. Plasma diluted 1:2 was used to detect cytokines and chemokines by use of the 31-Plex Cytokine/Chemokine array (Eve Technologies).

Isolation and Culturing of Primary Embryonic Neurospheres. Cortical regions of embryos (E13.5–14.5) were dissected. Tissues were dissociated with 0.05% trypsin/EDTA, and then titrated through a 40-μm cell filter to ensure single cells. Cells were then centrifuged, resuspended in starting medium [DMEM/Ham's F-12 nutrient solution + GlutaMAX (no. 10565018; Gibco), 50 U/mL penicillin, 50 μg/mL streptomycin, 0.25 μg/mL amphotericin B (no. 15290018; Gibco), 2% B27 (no. 17504001; Thermo Fisher Scientific), 20 ng/mL EGF, and 10 ng/mL FGF2 (no. 028-EG-200 and no. 3139-FB-025/CF, respectively; R&D Systems)], and seeded at a density of 200,000 cells/mL. Cells were grown in starting medium at 37 °C, 5% CO_2. Half of the medium was changed every second day. After 7 d of growth, passage 1 neurospheres were dissociated using the NeuroCult Chemical Dissociation kit following the manufacturer's protocol (no. 05707; STEMCELL Technologies). Cells were resuspended in starting medium and seeded for continual growth or experiments.

EdU Incorporation. Single cells were seeded on coverslips in 24-well plates coated with poly-D-lysine (no. A-003-M; Sigma Aldrich) and laminin (no. L2020; Sigma Aldrich) (3×10^5 cells per well). One day after seeding, cells were treated with 1 mM NR (ChromaDex) or not treated. Twenty-two hours after NR treatment, 10 μM EdU (Invitrogen) was added to each well. Two hours later, the cells were fixed with 4% PFA, and EdU was visualized with the Click-iT EdU Imaging Kit (no. C10337; Invitrogen) following the manufacturer's protocol. The cells were then either mounted with DAPI mounting medium (no. P36062; Life Technologies) or additionally stained for Sox2 (no. AF2018; R&D Systems) to ensure a culture of neuronal progenitor cells. Quantification was performed using ImageJ.

Immunoblot Analysis. Mouse hippocampal lysates were prepared, and Western blot analyses were performed as described previously (12). Briefly, mouse hippocampi were collected and lysed in radioimmunoprecipitation assay (RIPA) buffer (no. 9806S; Cell Signaling) containing protease inhibitors (no. B14002; Bimake) and phosphatase inhibitors (no. B15002; Bimake). Proteins were separated on 4–12% Bis-Tris gel (no. NP0336BOX; Thermo Fisher Scientific) or 4–15% Criterion TGX precast midi protein gel (no. 5671085; Bio-Rad) and probed with antibodies. Antibodies used were PAR (no. 4336-BPC-100; Trevigen), PARP1 (no. 9542; Cell Signaling), β-actin (no. sc-1616; Santa Cruz), SIRT3 (no. 5490; Cell Signaling), SIRT6 (no. ab88494; Abcam), Bcl-2 (no. sc-7382; Santa Cruz), SOD2 (no. AD1-SOD-110-F; Enzo), acetylated SOD2 (no. 214675; Abcam), Tau (no. MN1000; Thermo Fisher Scientific), Tau-pSer^{202}+Thr^{205} (AT8, no. MN1020; Thermo Fisher Scientific), Tau-pThr^{231} (AT180, no. MN1040; Thermo Fisher Scientific), and Tau-pThr^{181} (AT270, no. MN1050; Thermo Fisher Scientific).

Statistical Analysis. GraphPad Prism 6.0 was used. The data are shown as the mean ± SEM. Group differences were analyzed with one-way or two-way ANOVA followed by the Tukey multiple comparisons test for comparison among multiple groups. The two-tailed unpaired *t* test was applied for comparisons between two groups. Differences were considered statistically significant when $P < 0.05$.

For other detailed materials and methods, see *SI Materials and Methods*.

ACKNOWLEDGMENTS. We thank Drs. Prabhat Khadka, Sarah Mitchell, and Hyundong Song for help in the experiments; Dr. Magdalena Misiak for preparing neurospheres; Elin Lehrmann and Kevin G. Becker for microarray technical support; and Drs. Beimeng Yang and Tyler Demarest for critical reading of the manuscript. This research was supported by the Intramural Research Program of the NIH (V.A.B.), the NIA, ChromaDex (V.A.B.), and a grant from NIA Post-Doctoral Fellowship Training and Career Development Funding Project (to Y.H.). The V.A.B. laboratory has a Cooperative Research and Development Agreement arrangement with ChromaDex.

1. Alzheimer's A; Alzheimer's Association (2016) 2016 Alzheimer's disease facts and figures. *Alzheimers Dement* 12:459–509.
2. Hardy J, Selkoe DJ (2002) The amyloid hypothesis of Alzheimer's disease: Progress and problems on the road to therapeutics. *Science* 297:353–356.
3. Selkoe DJ (2002) Deciphering the genesis and fate of amyloid beta-protein yields novel therapies for Alzheimer disease. *J Clin Invest* 110:1375–1381.
4. Hou Y, Song H, Croteau DL, Akbari M, Bohr VA (2017) Genome instability in Alzheimer disease. *Mech Ageing Dev* 161:83–94.
5. Wyss-Coray T (2006) Inflammation in Alzheimer disease: Driving force, bystander or beneficial response? *Nat Med* 12:1005–1015.
6. Kerr JS, et al. (2017) Mitophagy and Alzheimer's disease: Cellular and molecular mechanisms. *Trends Neurosci* 40:151–166.
7. Bonkowski MS, Sinclair DA (2016) Slowing ageing by design: The rise of NAD+ and sirtuin-activating compounds. *Nat Rev Mol Cell Biol* 17:679–690.
8. Cantó C, Menzies KJ, Auwerx J (2015) NAD(+) metabolism and the control of energy homeostasis: A balancing act between mitochondria and the nucleus. *Cell Metab* 22: 31–53.
9. Verdin E (2015) NAD^+ in aging, metabolism, and neurodegeneration. *Science* 350: 1208–1213.
10. Cantó C, Sauve AA, Bai P (2013) Crosstalk between poly(ADP-ribose) polymerase and sirtuin enzymes. *Mol Aspects Med* 34:1168–1201.
11. Fang EF, et al. (2014) Defective mitophagy in XPA via PARP-1 hyperactivation and NAD(+)/SIRT1 reduction. *Cell* 157:882–896.
12. Fang EF, et al. (2016) NAD+ replenishment improves lifespan and healthspan in ataxia telangiectasia models via mitophagy and DNA repair. *Cell Metab* 24:566–581.
13. Long AN, et al. (2015) Effect of nicotinamide mononucleotide on brain mitochondrial respiratory deficits in an Alzheimer's disease-relevant murine model. *BMC Neurol* 15:19.
14. Wang X, Hu X, Yang Y, Takata T, Sakurai T (2016) Nicotinamide mononucleotide protects against β-amyloid oligomer-induced cognitive impairment and neuronal death. *Brain Res* 1643:1–9.
15. Birkmayer JG, Vrecko C, Volc D, Birkmayer W (1993) Nicotinamide adenine dinucleotide (NADH)–A new therapeutic approach to Parkinson's disease. Comparison of oral and parenteral application. *Acta Neurol Scand Suppl* 146:32–35.
16. Liu D, et al. (2013) Nicotinamide forestalls pathology and cognitive decline in Alzheimer mice: Evidence for improved neuronal bioenergetics and autophagy procession. *Neurobiol Aging* 34:1564–1580.
17. Scheibye-Knudsen M, et al. (2014) A high-fat diet and NAD(+) activate Sirt1 to rescue premature aging in cockayne syndrome. *Cell Metab* 20:840–855.
18. Zhang H, et al. (2016) NAD^+ repletion improves mitochondrial and stem cell function and enhances life span in mice. *Science* 352:1436–1443.
19. Jeppesen DK, Bohr VA, Stevnsner T (2011) DNA repair deficiency in neurodegeneration. *Prog Neurobiol* 94:166–200.
20. Obulesu M, Rao DM (2010) DNA damage and impairment of DNA repair in Alzheimer's disease. *Int J Neurosci* 120:397–403.
21. Wang J, Markesbery WR, Lovell MA (2006) Increased oxidative damage in nuclear and mitochondrial DNA in mild cognitive impairment. *J Neurochem* 96:825–832.
22. Bradley-Whitman MA, et al. (2014) Nucleic acid oxidation: An early feature of Alzheimer's disease. *J Neurochem* 128:294–304.
23. Lovell MA, Markesbery WR (2007) Oxidative DNA damage in mild cognitive impairment and late-stage Alzheimer's disease. *Nucleic Acids Res* 35:7497–7504.
24. Chow HM, Herrup K (2015) Genomic integrity and the ageing brain. *Nat Rev Neurosci* 16:672–684.
25. Martire S, Mosca L, d'Erme M (2015) PARP-1 involvement in neurodegeneration: A focus on Alzheimer's and Parkinson's diseases. *Mech Ageing Dev* 146–148:53–64.
26. Martire S, et al. (2016) Bioenergetic impairment in animal and cellular models of Alzheimer's disease: PARP-1 inhibition rescues metabolic dysfunctions. *J Alzheimers Dis* 54:307–324.
27. Sykora P, et al. (2013) Modulation of DNA base excision repair during neuronal differentiation. *Neurobiol Aging* 34:1717–1727.
28. Wei W, Englander EW (2008) DNA polymerase beta-catalyzed-PCNA independent long patch base excision repair synthesis: A mechanism for repair of oxidatively damaged DNA ends in post-mitotic brain. *J Neurochem* 107:734–744.
29. Weissman L, et al. (2007) Defective DNA base excision repair in brain from individuals with Alzheimer's disease and amnestic mild cognitive impairment. *Nucleic Acids Res* 35:5545–5555.
30. Copani A, et al. (2006) DNA polymerase-beta is expressed early in neurons of Alzheimer's disease brain and is loaded into DNA replication forks in neurons challenged with beta-amyloid. *J Neurosci* 26:10949–10957.
31. Patterson D, Cabelof DC (2012) Down syndrome as a model of DNA polymerase beta haploinsufficiency and accelerated aging. *Mech Ageing Dev* 133:133–137.
32. Raji NS, Rao KS (1998) Trisomy 21 and accelerated aging: DNA-repair parameters in peripheral lymphocytes of Down's syndrome patients. *Mech Ageing Dev* 100:85–101.
33. Oddo S, et al. (2003) Triple-transgenic model of Alzheimer's disease with plaques and tangles: Intracellular Abeta and synaptic dysfunction. *Neuron* 39:409–421.
34. Jankowsky JL, et al. (2004) Mutant presenilins specifically elevate the levels of the 42 residue beta-amyloid peptide in vivo: Evidence for augmentation of a 42-specific gamma secretase. *Hum Mol Genet* 13:159–170.
35. Sykora P, et al. (2015) DNA polymerase β deficiency leads to neurodegeneration and exacerbates Alzheimer disease phenotypes. *Nucleic Acids Res* 43:943–959.
36. Misiak M, et al. (2016) DNA polymerase beta decrement triggers death of olfactory bulb cells and impairs olfaction in a mouse model of Alzheimer's disease. *Aging Cell* 16:162–172.
37. Trammell SA, et al. (2016) Nicotinamide riboside is uniquely and orally bioavailable in mice and humans. *Nat Commun* 7:12948.
38. Frederick DW, et al. (2016) Loss of NAD homeostasis leads to progressive and reversible degeneration of skeletal muscle. *Cell Metab* 24:269–282.
39. Mendelsohn AR, Larrick JW (2014) Partial reversal of skeletal muscle aging by restoration of normal NAD^+ levels. *Rejuvenation Res* 17:62–69.
40. Mazoteras Muñoz V, et al. (2010) Gait and balance impairments in Alzheimer disease patients. *Alzheimer Dis Assoc Disord* 24:79–84.
41. O'Brien RJ, et al. (2009) Neuropathologic studies of the Baltimore Longitudinal Study of Aging (BLSA). *J Alzheimers Dis* 18:665–675.
42. Kashiwaya Y, et al. (2013) A ketone ester diet exhibits anxiolytic and cognition-sparing properties, and lessens amyloid and tau pathologies in a mouse model of Alzheimer's disease. *Neurobiol Aging* 34:1530–1539.
43. Kim SY, Volsky DJ (2005) PAGE: Parametric analysis of gene set enrichment. *BMC Bioinformatics* 6:144.
44. Ogata H, et al. (1999) KEGG: Kyoto encyclopedia of genes and genomes. *Nucleic Acids Res* 27:29–34.
45. Fabregat A, et al. (2016) The Reactome pathway Knowledgebase. *Nucleic Acids Res* 44:D481–D487.
46. Kandel ER (2001) The molecular biology of memory storage: A dialogue between genes and synapses. *Science* 294:1030–1038.
47. Lie DC, Song H, Colamarino SA, Ming GL, Gage FH (2004) Neurogenesis in the adult brain: New strategies for central nervous system diseases. *Annu Rev Pharmacol Toxicol* 44:399–421.
48. Subramanian S, et al. (2010) CCR6: A biomarker for Alzheimer's-like disease in a triple transgenic mouse model. *J Alzheimers Dis* 22:619–629.
49. Spillantini MG, Goedert M (2013) Tau pathology and neurodegeneration. *Lancet Neurol* 12:609–622.
50. Buerger K, et al. (2002) Differential diagnosis of Alzheimer disease with cerebrospinal fluid levels of tau protein phosphorylated at threonine 231. *Arch Neurol* 59: 1267–1272.
51. Guarente L (2016) CELL METABOLISM. The resurgence of NAD^+. *Science* 352: 1396–1397.
52. Ramamoorthy M, et al. (2012) Sporadic Alzheimer disease fibroblasts display an oxidative stress phenotype. *Free Radic Biol Med* 53:1371–1380.
53. Croteau DL, Bohr VA (1997) Repair of oxidative damage to nuclear and mitochondrial DNA in mammalian cells. *J Biol Chem* 272:25409–25412.
54. Herceg Z, Wang ZQ (2001) Functions of poly(ADP-ribose) polymerase (PARP) in DNA repair, genomic integrity and cell death. *Mutat Res* 477:97–110.
55. Cheng A, et al. (2016) Mitochondrial SIRT3 mediates adaptive responses of neurons to exercise and metabolic and excitatory challenges. *Cell Metab* 23:128–142.
56. Brown KD, et al. (2014) Activation of SIRT3 by the NAD^+ precursor nicotinamide riboside protects from noise-induced hearing loss. *Cell Metab* 20:1059–1068.
57. Gong B, et al. (2013) Nicotinamide riboside restores cognition through an upregulation of proliferator-activated receptor-γ coactivator 1α regulated β-secretase 1 degradation and mitochondrial gene expression in Alzheimer's mouse models. *Neurobiol Aging* 34:1581–1588.
58. Ryu D, et al. (2016) NAD+ repletion improves muscle function in muscular dystrophy and counters global PARylation. *Sci Transl Med* 8:361ra139.
59. Kaluski S, et al. (2017) Neuroprotective functions for the histone deacetylase SIRT6. *Cell Rep* 18:3052–3062.
60. Serrano-Pozo A, et al. (2013) Differential relationships of reactive astrocytes and microglia to fibrillar amyloid deposits in Alzheimer disease. *J Neuropathol Exp Neurol* 72:462–471.
61. Lee HJ, Hong YS, Jun W, Yang SJ (2015) Nicotinamide riboside ameliorates hepatic metaflammation by modulating NLRP3 inflammasome in a rodent model of type 2 diabetes. *J Med Food* 18:1207–1213.
62. Trammell SA, et al. (2016) Nicotinamide riboside opposes type 2 diabetes and neuropathy in mice. *Sci Rep* 6:26933.
63. Love S, Barber R, Wilcock GK (1999) Increased poly(ADP-ribosyl)ation of nuclear proteins in Alzheimer's disease. *Brain* 122:247–253.
64. Vorhees CV, Williams MT (2006) Morris water maze: Procedures for assessing spatial and related forms of learning and memory. *Nat Protoc* 1:848–858.
65. Leger M, et al. (2013) Object recognition test in mice. *Nat Protoc* 8:2531–2537.
66. Ghosal K, et al. (2009) Alzheimer's disease-like pathological features in transgenic mice expressing the APP intracellular domain. *Proc Natl Acad Sci USA* 106: 18367–18372.
67. Curzon P, Rustay NR, Browman KE (2009) Cued and contextual fear conditioning for rodents. *Methods of Behavior Analysis in Neuroscience*, Frontiers in Neuroscience, ed Buccafusco JJ (CRC, Boca Raton, FL), 2nd Ed.
68. Zhang J, et al. (2011) The AAA+ ATPase thorase regulates AMPA receptor-dependent synaptic plasticity and behavior. *Cell* 145:284–299.